

## Article

# Facile Synthesis and the Thermal Properties of Al/Si Composites Prepared via Fast Hot-Pressing Sintering

Jianping Jia <sup>1,\*</sup>, Xiaoxuan Hei <sup>2</sup>, Zhou Li <sup>3</sup>, Wei Zhao <sup>3</sup> , Yuqi Wang <sup>3</sup>, Qing Zhuo <sup>3</sup>, Hangyu Dong <sup>3,4</sup> , Yuanyuan Li <sup>3,4</sup>, Futian Liu <sup>2,\*</sup> and Yingru Li <sup>3,4,\*</sup> 

<sup>1</sup> Faculty of Science, Yibin University, Yibin 644007, China

<sup>2</sup> School of Materials Science and Engineering, University of Jinan, Jinan 250000, China; heix1125@163.com

<sup>3</sup> College of Intelligent Systems Science and Engineering, Hubei Minzu University, Enshi 445000, China; 2000048@hbmzu.edu.cn (Z.L.); 202230510@hbmzu.edu.cn (W.Z.); 202230511@hbmzu.edu.cn (Y.W.); 202330293@hbmzu.edu.cn (Q.Z.); 2022011@hbmzu.edu.cn (H.D.); 2023026@hbmzu.edu.cn (Y.L.)

<sup>4</sup> Key Laboratory of Green Manufacturing of Super-Light Elastomer Materials of State Ethnic Affairs Commission, Hubei Minzu University, Enshi 445000, China

\* Correspondence: windstears@sina.com (J.J.); mse\_liuft@ujn.edu.cn (F.L.); 2020030@hbmzu.edu.cn (Y.L.)

**Abstract:** In this paper, a novel power sintering technique, named fast hot-pressing sintering (FHP), which is able to achieve an ultrahigh heating rate similar to the spark plasma sintering (SPS) technique, but at a much lower cost, was applied to prepare a series of Al/Si composites with different Si volume ratios (12 vol.% to 70 vol.%) to meet the requirements of advanced packaging materials for electronic devices. In contrast to SPS, the FHP oven possesses a safe and budget-friendly current power supply, rather than a complex and expensive pulse power supply, for its heating power. The optimized sintering parameters (temperature, pressure and holding time) of FHP for preparing Al/Si composites were investigated and determined as 470 °C, 300 MPa and 5 min, respectively. In order to characterize the potential of Al/Si composites as packaging materials, thermal conductivities and coefficients of thermal expansion were studied. The thermal conductivity of the Al-40Si composite sintered by the FHP method is higher than that of the conventional SPS method (139 to 107 W m<sup>-1</sup> K<sup>-1</sup>). With the increase in Si, the thermal conductivities and coefficients of thermal expansion on both decreases. Furthermore, the thermal conductivities obey the Agari model, whereas the coefficient of thermal expansion and Si volume ratios obey additivity. The numeric modeling would help develop required packaging materials based on the thermal performances of the substrate materials, like Si or GaAs semiconductor devices.

**Keywords:** Al/Si composites; fast hot pressing sintering; packaging material; thermal conductivity; coefficient of thermal expansion



**Citation:** Jia, J.; Hei, X.; Li, Z.; Zhao, W.; Wang, Y.; Zhuo, Q.; Dong, H.; Li, Y.; Liu, F.; Li, Y. Facile Synthesis and the Thermal Properties of Al/Si Composites Prepared via Fast Hot-Pressing Sintering. *Metals* **2023**, *13*, 1787. <https://doi.org/10.3390/met13101787>

Academic Editor: Francisco Paula Gómez Cuevas

Received: 10 September 2023

Revised: 2 October 2023

Accepted: 6 October 2023

Published: 22 October 2023



**Copyright:** © 2023 by the authors. Licensee MDPI, Basel, Switzerland. This article is an open access article distributed under the terms and conditions of the Creative Commons Attribution (CC BY) license (<https://creativecommons.org/licenses/by/4.0/>).

## 1. Introduction

With the development of the semiconductor and microelectronics industries, microelectronic devices are developing towards miniaturization, high performance and high-power consumption, meaning that the heat generated is multiplied, which puts forward new requirements for thermal management materials with enhanced and comprehensive thermal performances [1–5]. Electronic packaging materials play an important role in heat dissipation of microelectronic devices, and nearly 30% of the current microelectronic performances are limited by electronic packaging materials [6]. An ideal electronic packaging material should have a high thermal conductivity (>100 W m<sup>-1</sup> K<sup>-1</sup>) to maximize heat dissipation [6,7]. Meanwhile, it should possess a lower coefficient of thermal expansion, which can be tailored in a wide range (7~16 K<sup>-1</sup>) to match the substrate material, like Si or GaAs semiconductor devices, in order to reduce the thermal stress and fatigue in the working conditions [6,8]. In addition, low density is also a favorable property that should

be taken into consideration for packaging materials. However, traditional packaging materials, including Al, Cu, Cu-W, C-Mo, and Kovar alloys, have difficulty satisfying the requirements of advanced electronic applications [9,10]. For instance, pure Al possesses favorable thermal conductivity as high as  $217 \text{ W m}^{-1} \text{ K}^{-1}$ , but suffers a unacceptable coefficient of thermal expansion of  $23.2 \text{ K}^{-1}$ , which limits the utilization of pure Al in advanced electronic applications [11–13].

Aluminum matrix composites as packaging materials have been widely investigated for their good economy and processability [14]. By adding high fractions of particle additives with low coefficients of thermal expansion, the thermal expansion behavior of the composites would be restricted significantly [4,7,9,15–18]. Meanwhile, the thermal conductivity of the composites can also be improved, or at least remain within acceptable values. The influences of adding diamond [19–24], TiC [17],  $\text{Si}_3\text{N}_4$  [25], cBN [16], or SiC [10,18,26–28] via different techniques on the thermal behaviors of aluminum matrix composites were deeply studied. Recently, Si particles were suggested to be a potential additive for aluminum matrix composites due to their low coefficients of thermal expansion, high thermal conductivity and low density [7–9,15,29–31]. Moreover, superior to other ceramic additives like SiC, diamond and  $\text{Si}_3\text{N}_4$ , Al/Si composites demonstrate a much lower cost and good recyclability, since Al/Si composites can be recycled and processed into Al-Si alloys, which are a series of cast Al alloys widely used in the structural parts of machines. A variety of methods are adopted to prepare Al/Si composites, including squeeze casting [32,33], gas-pressured infiltration [34], vacuum pressure infiltration [35–37], spray atomization and deposition [38], spark plasma sintering (SPS) [15,16,22–24,39], hot pressing [40–42], etc. These methods can be classified into two categories: powder metallurgy and liquid phase methods. Generally, liquid phase methods are cheaper, but it is difficult to prepare high-density Al/Si composites with high fractions of Si compared with powder metallurgy represented by SPS. SPS is identified as a non-conventional powder consolidation method, which employs electric current directly through the powders. By discharging between the powder particles, it can produce spark plasma and high local temperatures, making some components soften or even partially melt and then fill the spaces between other particles and integrate together. Thus, SPS is very suitable for preparing high-density composites composed of matrixes and reinforced phases with significantly different melting points, including Al/Si composite systems. However, SPS ovens usually possess complex and expensive pulse power supplies and corresponding controlling systems, which make SPS ovens huge and expensive, and not beneficial for large-scale industrial production. New powder metallurgy sintering techniques and new equipment are still strongly in demand.

In this paper, a novel powder sintering technique developed by our group, named fast hot-pressing sintering (FHP), was employed to prepare Al/Si composites with a wide Si volume ratio. FHP can also achieve an ultrahigh heating rate, similar to the SPS technique, to satisfy the special requirements of Al and Si powder sintering. In the meanwhile, compared with SPS method, no complex and expensive pulse power supply is employed in the design of FHP, which made the cost of the FHP oven less than a quarter of that of the SPS oven with the same processing capability. The optimized FHP sintering parameters to prepare Al/Si composite samples via the FHP technique were determined first, and the thermal performances of Al/Si composite samples with Si volume ratios of 12 vol.%, 27 vol.%, 40 vol.%, 50 vol.% and 70 vol.% were studied. Kinds of thermal conductivity models are employed to investigate the relationship between Si volume ratios and thermal performances. The results show that thermal performances of the Al/Si composite prepared via the FHP technique are comparable with those prepared via the SPS technique. Given its economy, FHP is believed to be a promising technique to prepare Al/Si composite packaging material for electronic devices.

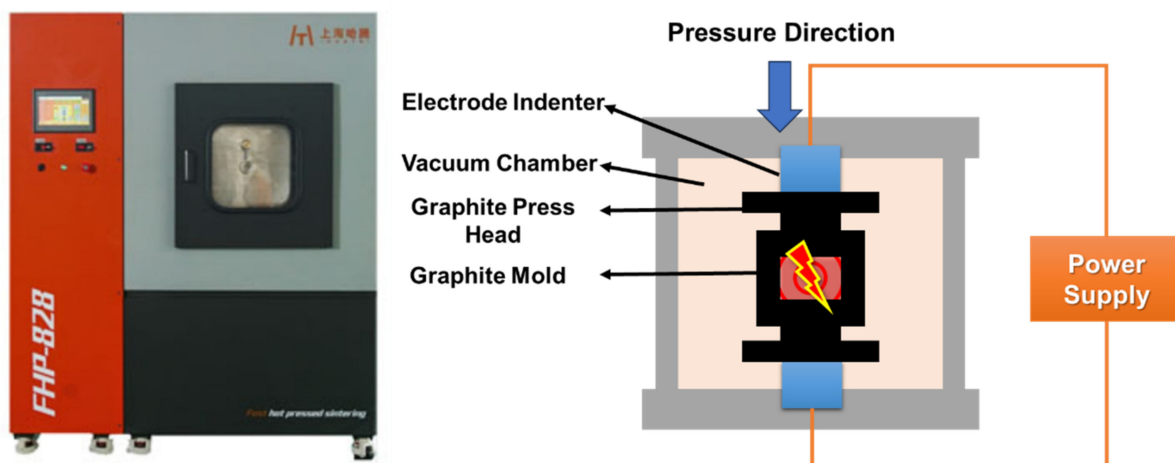
## 2. Materials and Experiments

### 2.1. Materials

Pure Al powders with particle sizes of around 100  $\mu\text{m}$  were purchased from SCM Metal Products, Inc (Suzhou, China), and pure Si powders with particle sizes of around 10  $\mu\text{m}$  were purchased from Ruiteng Alloy Materials Co. Ltd. (Nangong, China).

### 2.2. Synthesis of Al/Si Composites via Fast Hot-Pressing Sintering

The Al/Si composites with different component were sintered via a fast hot-pressing sintering oven (FHP-828, Haaten Technology Co. Ltd., Suzhou, China). The FHP technique is designed by Dr. Jianping Jia and originated from Haaten Technology Co. Ltd, Suzhou, China. The scheme of the fast hot-pressing sintering oven is shown in Scheme 1. The core part of the FHP oven includes a vacuum chamber, a high voltage direct current power supply, a pair of electrode indenters, and an appropriate mold (usually made of graphite or hard alloy). In the FHP technique, the material is directly heated up by use of a direct current at an ultrahigh heating rate of up to 1000  $^{\circ}\text{C min}^{-1}$ , under the high pressure provided by the indenter. In summary, the sintering time in the FHP technique is much shorter than that of the traditional vacuum hot-pressing method, and comparable with SPS. Meanwhile, the FHP oven possesses some advantages compared to the SPS equipment, such as a low economic cost, simple design, small volume, ease of maintenance, the simplicity of automatic production, etc., which make FHP a promising technique to prepare advanced materials via the powder sintering route, including advanced metals or alloys, ceramics, and complex composites.



**Scheme 1.** The FHP-828 oven and a scheme of the core part of the FHP oven.

Typically, the Al/Si composite samples are disk shaped ( $\Phi 12 \times 2\sim 3$  mm) and prepared with the following procedures: (1) Al powders and Si powders with different volume ratios (the Si volume ratios are 12 vol.%, 27 vol.%, 40 vol.%, 50 vol.% and 70 vol.%, respectively, and the corresponding samples are named Al-12Si, Al-27Si, Al-40Si, Al-50Si, Al-70Si) were mixed thoroughly, and then added into the hard alloy mold lined with graphite paper, followed by sufficient shaking of the mold to make the powders mix homogeneously; (2) the mold was transferred to the press machine for pre-pressing to ensure the powders would not spill out of the mold; and (3) the mold was, at last, transferred to the FHP oven, and when the vacuum degree was lower than 10 Pa, the temperature and press program started. The program was performed as follows: (1) firstly, the press program started, and the pressure came up to the settled value within 1 min (Table 1); (2) the temperature program started successively, and the heating rate was set to 100  $^{\circ}\text{C min}^{-1}$  until the temperature of the mold reached 100  $^{\circ}\text{C}$  below the target temperature; (3) then the heating rate was changed to 50  $^{\circ}\text{C min}^{-1}$  until the temperature of the mold reached to the target temperature;

(4) the temperature and pressure are maintained for certain time; and (5) after cooling with the FHP-828 oven, the Al/Si composite samples were finally prepared.

**Table 1.** Details of the experiments for optimization of the FHP sintering parameters.

Experiment Series	Sintering Temperature (°C)	Sintering Pressure (MPa)	Holding Time (Min)
Series 1	440	300	5
	450		
	460		
	470		
	475		
Series 2	470	100	5
		150	
		200	
		250	
		300	
Series 3	470	300	0
			5
			10
			15
			20

In order to determine the optimized FHP sintering parameters, Al-70Si was chosen as the representative sample, and 3 series of orthogonal experiments were carried out to find the optimized sintering temperature, sintering pressure and holding time. These parameters show great influence on the real density, which would surely affect the thermal properties. The details of experiments are exhibited in Table 1.

The Al/Si composite samples need some after-treatment before further characterizations. The graphite paper stuck to the surface of the samples was removed by sandblasting. Then, the samples were polished by polishing machine (YMPZ-2-300, Metallurgical Equipment Co. Ltd., Shanghai, China) with sandpapers of 400, 800 and 1200 mesh in succession. At last, the Al/Si composite samples were polished with a polishing cloth with a nano-diamond suspension, and samples with a metallic luster were finally obtained. An Al/Si composite disk sample with 70 vol.% Si is shown in Figure 1.



**Figure 1.** Photograph of an Al/Si composite disk sample with 70 vol.% Si.

### 2.3. Characterization

The real densities of samples were measured with a densitometer (PMDT AR-150PM, Hongtuo Equipment Co. Ltd., Dongguan, China). The relative density is calculated by dividing the real density by the theoretical density based on the densities of pure Al and Si together with the volume ratio. The microscopic morphology was examined by scanning

electronic microscopy (SEM, S-4800, Hitachi, Japan). The crystal structures were studied with an X-ray diffractometer (XRD, D/MAX-2500, Rigaku, Japan).

The thermal diffusivity ( $\alpha$ ,  $\text{m}^2 \text{s}^{-1}$ ) was measured with a laser flash Analyzer (LFA 467 HyperFlash, NETZSCH Analyzing & Testing, Selb, Germany). The specific heat capacity ( $C_p$ ,  $\text{J kg}^{-1} \text{K}^{-1}$ ) was measured with a differential scanning calorimeter (DSC 214, NETZSCH Analyzing & Testing, Selb, Germany). Thus, the thermal conductivity ( $k$ ,  $\text{W m}^{-1} \text{K}^{-1}$ ) could be calculated with Equation (1):

$$k = \alpha \times C_p \times \rho_r \quad (1)$$

where  $\rho_r$  is the real density of Al/Si composite sample measured by densitometer.

The coefficient of thermal expansion (CTE) was measured by a dilatometer (DIL 402C, NETZSCH Analyzing & Testing, Selb, Germany). The samples were cuboid shaped, with a size of  $4 \times 4 \times 25$  mm, prepared with the same procedures of Section 2.2. The testing temperature was set as room temperature, and the testing atmosphere was high pure nitrogen.

### 3. Results and Discussion

#### 3.1. Optimization of FHP Sintering Process

The parameters of the sintering process, including the sintering temperature, pressure, holding time, etc., play crucial roles in the successful preparation of powder-sintered products. During the sintering of Al/Si composites with different ratios, it was observed that the size and density of the pores inside the sintered material gradually decreased with the increase in Si content. In order to minimize the influence of porosity on the sintering quality, the samples with the highest silicon content (70 vol.%, no pores observed) were selected as the representative to adjust the sintering parameters of FHP method. The orthogonal experiments were carried out to study the influences of sintering temperature, pressure and holding time on the properties of the as-prepared Al-70Si samples.

##### 3.1.1. Sintering Temperature

The sintering temperature is one of the most important factors to control the softening and flowability of the powders (i.e., the plastic deformation ability), which would further affect the final density. As can be seen in Figure 2a, the density increases with the sintering temperature up to the temperature of 470 °C, and then decreases. The highest density reaches  $2.44 \text{ g cm}^{-3}$  at 470 °C. The softening temperature of pure Al is about 300 °C, and the plastic deformation ability of Al increases with the temperature. Meanwhile, Si has a much higher melting point of 1410 °C, resulting in Si particles not possessing plastic deformation abilities under the sintering temperature. Hence, it should be noted here that Al forms the continuous phase and Si forms the dispersed phase in the Al/Si composite prepared in this work. In the initial stage, a greater plastic deformation ability makes the Al powders more easily to bind with the Si powders and integrate together, which would increase the density of the Al/Si composite and ensure the thermal conductivity of the final product. The fluidity of Al increases gradually with the sintering temperature, allowing full contact of the Al/Si phases to reduce the sintering porosity. The decrease in porosity led to an increase in the density of the sintered bulk with a temperature increase in the range of 440–470 °C. However, the flowable Al would overflow from the gaps between molds under high pressure, due to its excessive fluidity induced by the high temperature (475 °C), which directly reduced the percentage of Al in the final sintered bulk. The loss of Al with a higher density ( $\rho_{\text{Al}} = 2.7 \text{ g cm}^{-3}$ ,  $\rho_{\text{Si}} = 2.33 \text{ g cm}^{-3}$ ) makes the density decrease slightly.

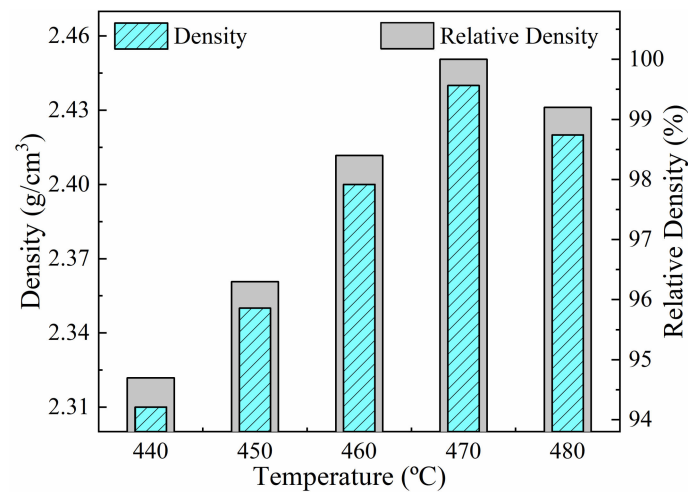


**Figure 2.** Influences of sintering temperature on density and relative density of Al-70Si composite samples. (The sintering pressure: 300 MPa, holding time: 5 min).

It is necessary to know the phase composition to calculate the theoretical density. Therefore, XRD analysis was employed (Figure 3). The XRD patterns of the Al-70Si composite samples prepared at different sintering temperatures are all composed of two groups of peaks, one for pure Al (JCPDS No. 04-0787), and the other for pure Si (JCPDS No. 27-1402), and no peaks related other phase in the phase diagram of Al-Si alloy can be observed, implying that no evidential solid solution phase was left after the FHP sintering. On the one hand, the solubilities of Al or Si in each other are both ultra-low at room temperature; on the other hand, even a temperature of 475 °C is far below the eutectic point of Al-Si system. Thus, it can be concluded that the Al-Si composites are almost composed of pure Al and Si, and the theoretical density could be directly calculated based on the volume ratio of Al and Si. Thus, the theoretical density of Al-70Si is calculated to be 2.441 g cm<sup>-3</sup>, and the highest relative density of the A-70Si sample prepared at 470 °C is nearly 100% (Figure 2b), implying that the densification of A-70Si can reach the limit when the sintering temperature is 470 °C.

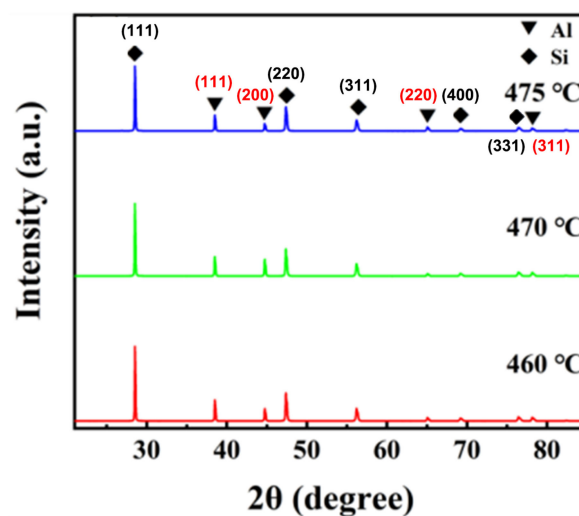


**Figure 3.** XRD patterns of Al-70Si composite samples prepared at sintering temperatures of 460 °C, 470 °C, 475 °C. (Sintering pressure: 300 MPa, holding time: 5 min).

SEM was employed to study the microscopic morphology of surfaces of the Al-70Si composite samples prepared at different sintering temperatures, in order to further evaluate the relationship between densification and sintering temperature (Figure 4). Cracks can

be clearly observed in the sample prepared at 450 °C, and as the sintering temperature increases, the number of cracks reduces and the size of cracks becomes small, suggesting that the integration between Al and Si is improved with the temperature increase. As a result, the density increases up to 470 °C. Therefore, a temperature of 470 °C should be the optimal sintering temperature.

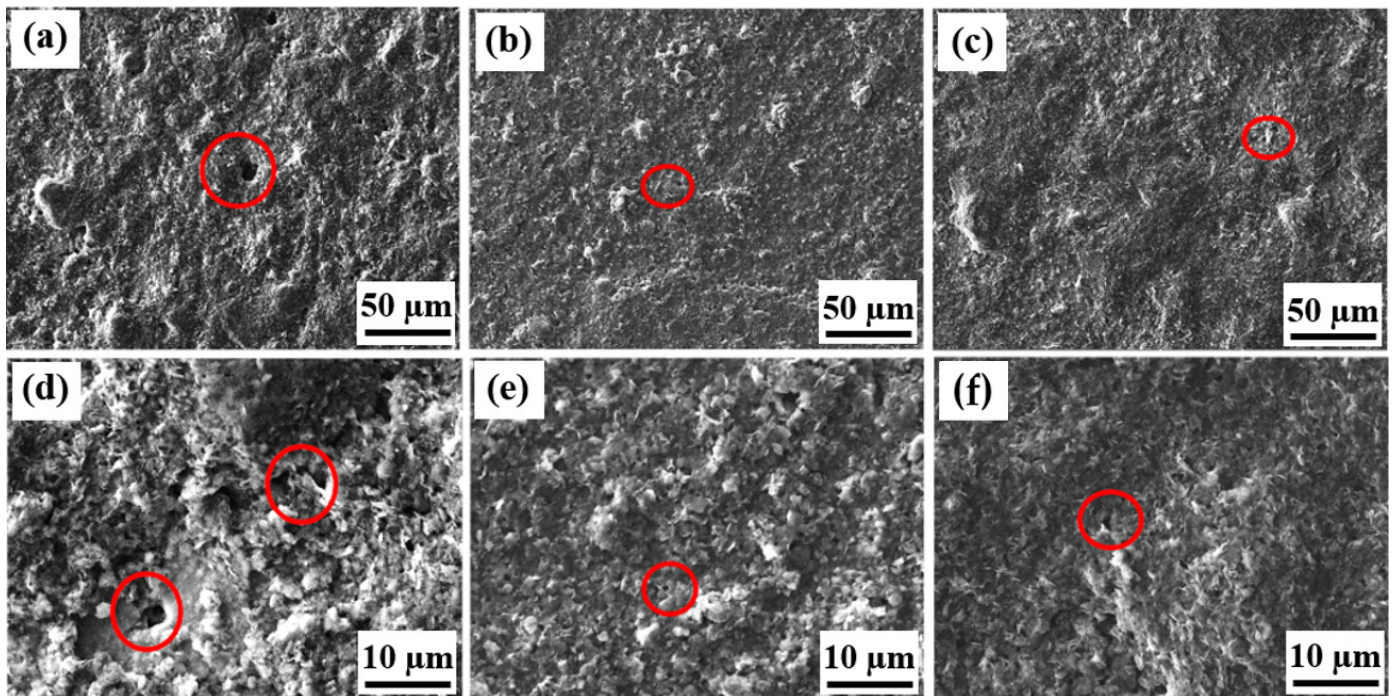


**Figure 4.** SEM images of Al-70Si composite samples prepared at sintering temperature of (a,d) 450 °C, (b,e) 460 °C, (c,f) 470 °C with different magnifications. (The sintering pressure: 300 MPa, holding time: 5 min. Cracks are marked with red circles).

### 3.1.2. Sintering Pressure

The sintering pressure shows great influence on the density in the powdering technique. Typically, in the powdering sintering technique, within the pressure limit that the mold can bear, the density will increase with the pressure. The Al-70Si composite prepared via the FHP technique also agrees with this regulation. The density keeps increasing from 100 MPa to 300 MPa, and the relative density reaches nearly 100% when the pressure arrives 300 MPa (Figure 5). As the sintering pressure increases, the contact between Al and Si powders becomes closer, which would decrease the resistance of the sample, and the current grows. Additionally, the plastic deformation ability of Al powders is also enhanced with the sintering temperature and the sintering current. As a result, the cracks disappear at a high sintering pressure, and the Al matrix becomes denser, which can be observed in the SEM images (Figure 6). XRD was also employed to study the microstructures of the samples prepared at different sintering pressures, and it is not unexpected that the XRD patterns share the same phase compositions; all are composed of nearly pure Al and pure Si (Figure 7). Given the security consideration, the experiment at a pressure higher than 300 MPa was not performed; moreover, the relative density of the sample prepared at 300 MPa is already able to satisfy production requirements. Thus, a pressure of 300 MPa should be the optimal sintering pressure.

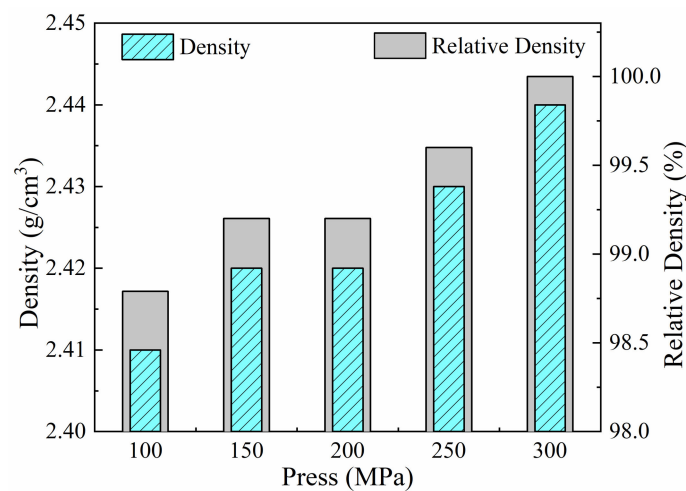


**Figure 5.** Influences of sintering pressure on density and relative density of Al-70Si composite samples. (The sintering temperature: 470 °C, holding time: 5 min).

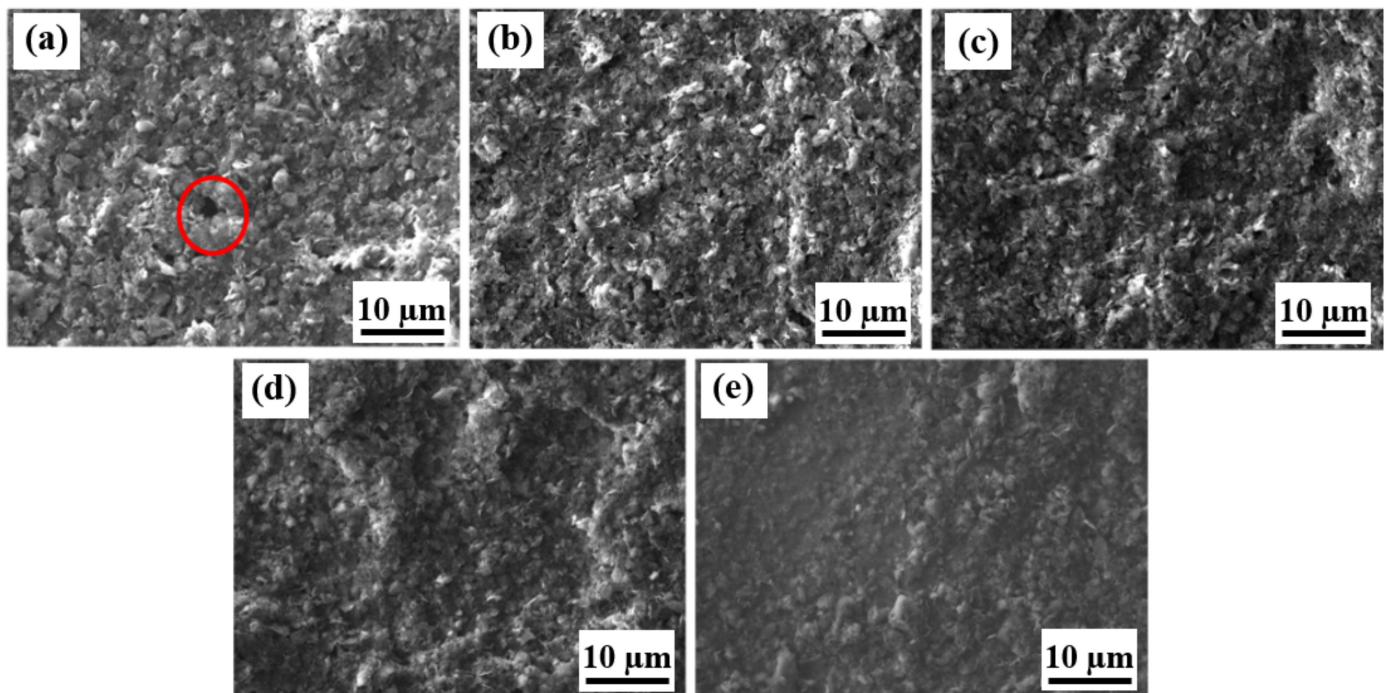


**Figure 6.** SEM images of Al-70Si composite samples prepared at sintering pressures of (a) 100 MPa, (b) 150 MPa, (c) 200 MPa, (d) 250 MPa, (e) 300 MPa. (The sintering temperature: 470 °C, holding time: 5 min. Cracks are marked with red circles).

### 3.1.3. Holding Time

The plastic deformation of Al powders during FHP sintering should necessarily take a certain time; thus, the holding time at sintering temperature would affect the densities of the final products, while a too long holding time is unfavorable to industrial production. Therefore, it is necessary to determine the suitable holding time. Several Al-70Si composite samples were prepared via the FHP technique with a holding time from 0–20 min under a sintering temperature of 470 °C and a sintering pressure of 300 MPa. Due to the rapid heating rate of 100 °C min<sup>-1</sup>, there are less than 2 min left for the plastic deformation of the Al particles during the heating process. As can be seen in Figure 8, the holding time of 0 min apparently does not provide enough time for the plastic deformation of Al particles. And, with a very short holding time of 5 min, the density has already reached 2.44 g cm<sup>-3</sup>,

and the relative density reaches nearly 100%. It would not show obvious influence on the density of the Al-70Si composite samples to further extend the holding time, because the holding treatment was designed to allow the continuous phase Al sufficient plastic deformation to encapsulate the dispersed phase Si at a high temperature and pressure. Under the corresponding sintering parameters (470 °C, 300 MPa), the process needed 5 min to be fully realized, at which time the density of the bulk is 2.44 g cm<sup>-3</sup> (100% relative density, i.e., ideal density). It will not change the physical mixing state of the two phases to continue increasing the holding time, nor will it induce a chemical reaction between the two phases to produce a new phase. Therefore, the density will not change. However, the microscopic morphology of the composites is affected by the holding time (Figure 9). No apparent aggregation of Si particles (given the high melting point of Si) can be seen in the cross-section SEM images for the sample with a holding time of 5 min. With an increase in the holding time, the aggregation of Si particles occurs, which is not beneficial to the overall performance of the Al/Si composite. Thus, 5 min should be the optimal holding time for sintering the Al/Si composite.

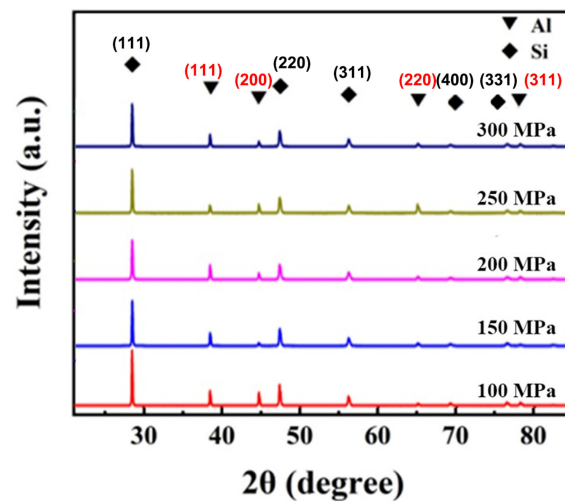


**Figure 7.** XRD patterns of Al-70Si composite samples prepared at different sintering pressure of 460 °C, 470 °C, 475 °C. (The sintering pressure: 300 MPa, holding time: 5 min).

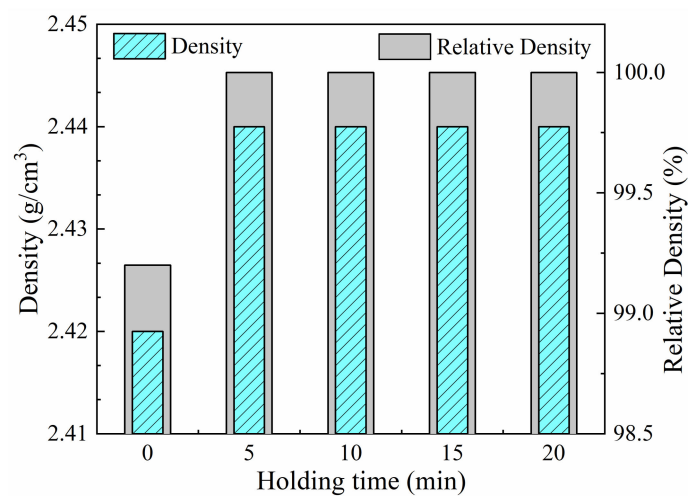


**Figure 8.** Influences of holding time on density and relative density of Al-70Si composite samples. (The sintering temperature: 470 °C, sintering pressure: 300 MPa).

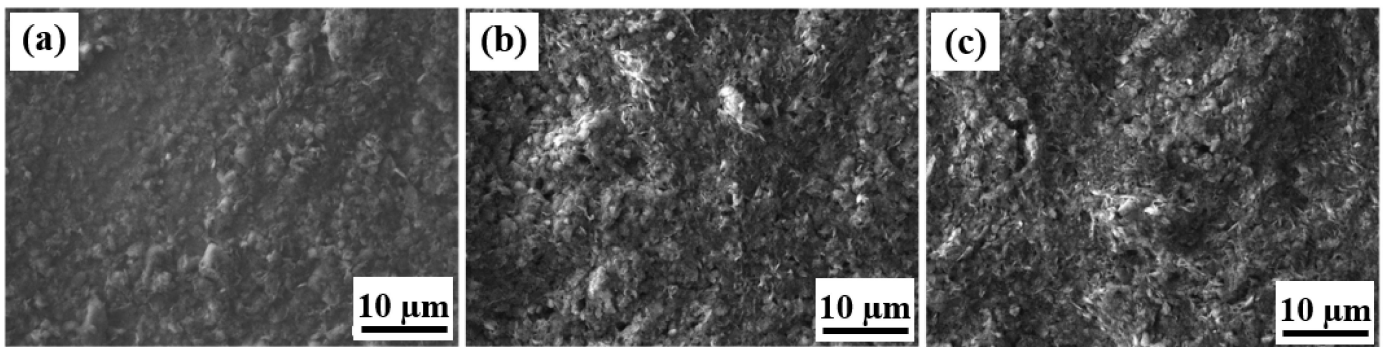


**Figure 9.** SEM images of Al-70Si composite samples prepared with holding time of (a) 5 min, (b) 10 min, (c) 20 min. (The sintering temperature: 470 °C, sintering pressure: 300 MPa).

To sum up, the optimized FHP sintering parameters for preparing the Al/Si composite are determined to be a sintering temperature of 470 °C, a sintering pressure of 300 MPa and holding time of 5 min. Hence, the rapid heating rate and short holding time ensure that the FHP sintering technique can be applied in large-scale industrial production of Al/Si composites for packaging materials. The samples for the following thermal analyses are all prepared under the above conditions.

### 3.2. Thermal Properties

The Al/Si composite is intended to be utilized as an electronic package material. Thus, the question of what proportion of Al and Si the thermal conductivity and coefficients of thermal expansion are acceptable should be answered. The Si volume ratios of Al/Si composite are controlled to be 12 vol.%, 27 vol.%, 40 vol.%, 50 vol.% and 70 vol.%, respectively, and the corresponding samples are named Al-12Si, Al-27Si, Al-40Si, Al-50Si and Al-70Si. These samples are all composed of two phases of Al and Si, as shown in the XRD patterns, and the differences in composition are reflected in the intensity of the peaks (Figure 10). As Al and Si form the continuous phase and dispersed phase, respectively, the higher the volume ratio of Al, the smoother the surface of the Al/Si composite samples becomes, as shown in the SEM images (Figure 11). Additionally, if the volume ratio of Si exceeds 50%, an obvious aggregation of Si particles can be observed (Figure 11d,e), which would also influence thermal properties. Thus, the differences in thermal properties are mainly affected by the ratio of Si and Al, rather than phase differences.

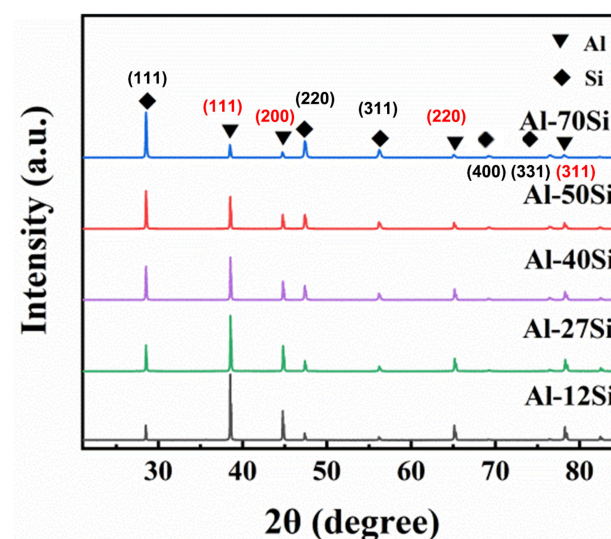


**Figure 10.** XRD patterns of Al-12Si, Al-27Si, Al-40Si, Al-50Si, Al-70Si.

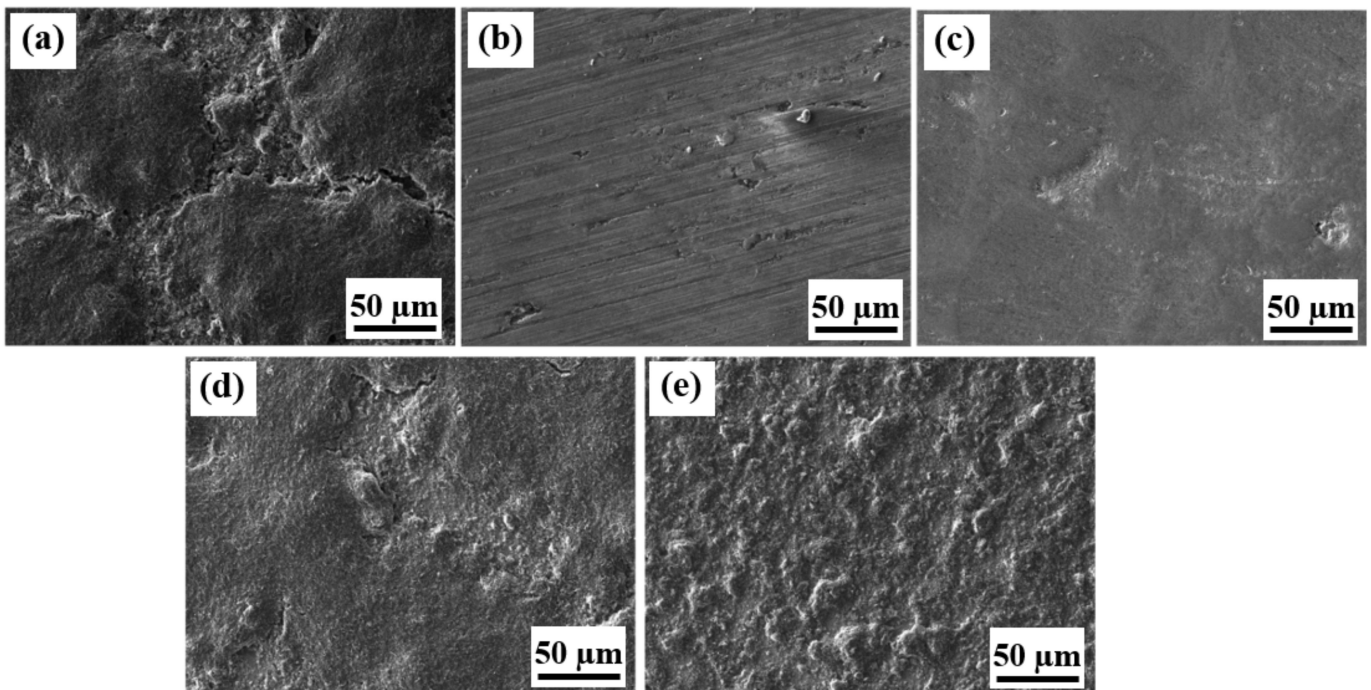


Figure 11. SEM images of (a) Al-12Si, (b) Al-27Si, (c) Al-40Si, (d) Al-50Si, (e) Al-70Si.

In order to satisfy the heat dissipation requirements for future high-performance processors, thermal conductivity is the primary consideration. The thermal conductivities of different Al/Si composite samples decrease as the volume ratio of Si increases (Figure 12). It should be pointed out that the theoretical thermal conductivities of pure Al and Si are  $217 \text{ W m}^{-1} \text{ K}^{-1}$  and  $148 \text{ W m}^{-1} \text{ K}^{-1}$ , respectively. When the volume ratio of Si exceeds 27 %, the thermal conductivities of the composites are already lower than that of pure Si, which is in the dispersed phase in the Al/Si composite. And the Al-70Si possesses the lowest thermal conductivity of  $98.2 \text{ W m}^{-1} \text{ K}^{-1}$ , less than half that of the thermal conductivity of pure Al. Two main reasons should contribute for the phenomenon: on the one hand, the increase in the volume ratio of Si, with a lower thermal conductivity and coefficient of thermal expansion, would inevitably lead to a decrease in thermal conductivity; on the other hand, the interface between the Al matrix and the Si particles is just formed through the plastic deformation of Al, and the tightly bonded alloy phase should not form at the boundary as described above, which goes against the interfacial thermal transfer and results in a higher interface thermal resistance.

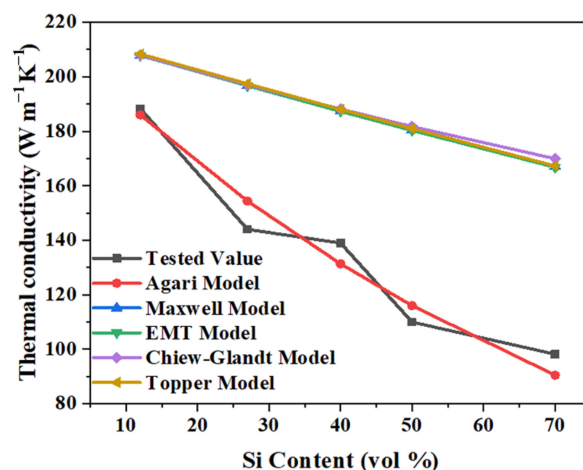


Figure 12. Thermal conductivities of different Al/Si composites.

In order to evaluate and predict the thermal conductivities of the Al/Si composites with different compositions for developing package materials with practical value, it is necessary to fit an empirical function between the volume ratio of Si and the thermal conductivity. Generally speaking, the thermal conductivity ( $k$ ) of a solid–solid binary composite is a function of the thermal conductivity of the continuous phase ( $k_c$ ), the thermal conductivity of the dispersed phase ( $k_d$ ), the volume ratio of the dispersed phase ( $\phi$ ), the shape and arrangement of the dispersed phase ( $a$ ), etc. Thus, the thermal conductivity generally has the following form:

$$k = k(k_c, k_d, \phi, a) \quad (2)$$

As the thermal conductivity is affected by numerous factors, much effort has been paid by many researchers to develop thermal conductivity models suitable for different systems, and to obtain a favorable function for a certain occasion is a complicated process indeed. The Al/Si composite in this work is also a kind of solid–solid binary composite system, and several widely applied theoretical and empirical models are discussed, including the Maxwell model [43,44], the EMT model [44], Chiew–Glandt model [45], the Topper model [46,47] and the Agari model [48,49]. The calculation formulae of the models are summarized in Table 2. As can be seen in Figure 12 and Table 3, the predictions of the Maxwell model, EMT model, the Chiew–Glandt model, and the Topper model are quite close, because the ratio of  $k_d$  and  $k_c$  ( $\kappa$ ) is calculated to be 0.682, relatively close to 1. But these predictions all deviate from the tested value greatly, suggesting that these four models are not suitable for predicting the thermal conductivities of Al/Si composites prepared via FHP sintering. The predictions of these four models are between the thermal conductivities of Al and Si. However, because of the widely distributed interfacial thermal resistance, when the volume ratio of Si exceeds 27%, the thermal conductivities of the composites are already lower than that of pure Si. Thus, the Maxwell model, the EMT model, the Chiew–Glandt model, and the Topper model failed to fit a matched curve based on the tested values. In contrast, the Agari model, with two adjustable parameters, can fit the tested values much better than other models, although the Agari model is generally applied to the systems of polymer–matrix composites. The parameters of  $C_1$  and  $C_2$  are fitted to be 0.995 and 0.829 by least squares method. Thus, the Agari model can be used to predict the thermal conductivities of Al/Si composite samples in a wide  $\phi$  to find the optimized package material.

**Table 2.** Calculation formulae of models applied in this work.

Calculation Model	Calculation Formula	Notes
Maxwell Model	$k = k_c \cdot \frac{\kappa + 2 + 2(\kappa - 1)\phi}{\kappa + 2 - (\kappa - 1)\phi}$	$\kappa$ is the ratio of $k_d$ and $k_c$ , $\kappa = \frac{k_d}{k_c}$
EMT Model	$k = k_c \cdot (\kappa A + \sqrt{\kappa^2 A^2 + \kappa/2})$	$A$ is an empirical parameter, $A = \frac{1}{4}(3\phi - 1 + \frac{2-3\phi}{\kappa})$
Chiew-Glandt Model	$k = k_c \cdot \frac{1 + 2\beta\phi + (2\beta^3 - 0.1\beta)\phi^2 + 0.05e^{4.5\beta}\phi^3}{1 - \beta\phi}$	$\beta$ is the reduced thermal polarizability, defined as $\beta = \frac{\kappa - 1}{\kappa + 2}$
Topper Model	$\frac{1}{k} = \frac{1 - \phi^{1/3}}{k_c} + \frac{\phi^{1/3}}{k_d\phi^{2/3} + k_c(1 - \phi^{2/3})}$	-
Agari Model	$\ln(k) = (1 - \phi)\ln(C_1 k_c) + \phi C_2 \ln(k_d)$	$C_1$ and $C_2$ are parameters fitted according to the tested values. In this paper, $C_1$ is fitted to be 0.995 and $C_2$ is fitted to be 0.829

The coefficient of thermal expansion (CTE) is another important thermal parameter for packaging materials. If the CTEs of packaging materials and substrate materials are not matched, the connection between them might be tortured during repeated thermal cycles, leading to a decline in the heat dissipation capabilities of the processor in its long-term life. The CTE of pure Al is  $23.2 \times 10^{-6} \text{ K}^{-1}$ , which is too large to be an appropriate packaging material alone. On the contrary, Si possesses a much smaller CTE of  $3.5 \times 10^{-6} \text{ K}^{-1}$ . Thus, since no alloy phase is generated during the FHP sintering process, the CTE is bound to

decline by adding a certain amount of Si, as shown in Figure 13. Additionally, the CTE of the Al/Si composite obeys the additivity simply, as shown in Equation (3).

$$\text{CTE} = (1 - \phi)\text{CTE}_{\text{Al}} + \phi\text{CTE}_{\text{Si}} \quad (3)$$

**Table 3.** Thermal conductivities of different Al/Si composites: tested values and calculated values based on different models.

Volume Ratio of Si	Thermal Conductivity ( $\text{W m}^{-1} \text{K}^{-1}$ )					
	Tested Value	Maxwell Model	EMT Model	Chiew-Glandt Model	Topper Model	Agari Model
12%	188.3	207.87	207.84	207.91	208.38	186.01
27%	144	196.81	196.69	197.06	197.45	154.39
40%	139	187.53	187.32	188.20	188.09	131.37
50%	110	180.57	180.31	181.76	181.01	116.02
70%	98.2	167.11	166.81	169.97	167.30	90.50

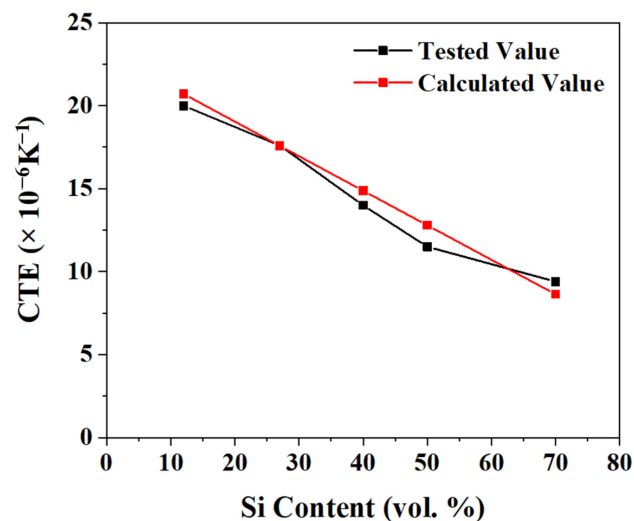


**Figure 13.** Coefficient of thermal expansion of different Al/Si composites.

To study the feasibility, reliability and advancement of the FHP technique, a comparison with other researchers' work on Al/Si composites prepared via the SPS technique is shown in Table 4. The thermal conductivities of Al/Si composites prepared via the FHP technique are comparable with those prepared via the SPS technique with a similar composition, and even higher than some reported values in others' studies. In the meanwhile, the coefficients of thermal expansion of the samples prepared via the FHP technique and the SPS technique with the same composition are quite close. The phenomena can be attributed to the fact that the reported samples of Al and Si composite system share the same phase constitution with the Al/Si composite in this paper.

To sum up, the thermal conductivity and the coefficient of thermal expansion of the Al/Si composite prepared via the FHP technique are investigated and fitted with the appropriate model, which makes it possible to develop suitable packaging materials of Al/Si composites based on the thermal properties of the substrate materials. A comparison of Al/Si composite systems prepared via SPS and FHP, respectively, shows that FHP is a novel sintering technique which can be compared to SPS. Given its remarkable economy, the FHP technique is bound to be a promising route for preparing Al/Si composites.

**Table 4.** Comparison of thermal properties of Al/Si composites in this paper and other Al-Si materials at room temperature.

No.	Material	Processing Method	$k$ (W m <sup>-1</sup> K <sup>-1</sup> )	CTE ( $\times 10^{-6}$ K <sup>-1</sup> )	Note
1	Al-45%Si	SPS	113	12.7	Ref [50]
2	Al-30%Si	SPS	114.4	14.57	Ref [6]
3	Al-40%Si	SPS	107.7	13.36	Ref [7]
4	Si(60%)/Al	SPS	116.5	9.8	Ref [8]
5	Al-27Si	FHP	144	17.6	This work
6	Al-40Si	FHP	139	14	This work
7	Al-50Si	FHP	110	11.5	This work

#### 4. Conclusions

In this paper, a novel powder sintering technique, FHP, was employed to prepare Al/Si composites with a wide range of Si volume ratios. The technique shows advantages of low costs, ultrahigh heating rates, good reliability and wide usability compared to the SPS technique. Additionally, the FHP oven is self-developed and self-produced. The sintering parameters were determined to be a sintering temperature of 470 °C, a sintering pressure of 300 MPa and a holding time of 5 min, after a series of orthogonal experiments. The relative density of the Al/Si composites can reach nearly 100%, suggesting the advantages of FHP sintering. The thermal performances of the Al/Si composite samples with Si volume ratios of 12 vol.%, 27 vol.%, 40 vol.%, 50 vol.% and 70 vol.% were studied. With an increase in the Si volume ratio, the thermal conductivities and the coefficients of thermal expansion both decrease, due to Si particles' thermal properties. Furthermore, different thermal conductivity models for solid–solid binary composites were employed to study the heat transfer behavior of Al/Si composites, and the Agari model is matched with the Al/Si system in this paper. The CTE of the Al/Si composites obey additivity simply. Numeric modeling would help develop the required packaging materials based on the thermal performances of the substrate materials, like Si or GaAs semiconductor devices. A side-by-side comparison between the FHP sintering method and the conventional SPS method was performed for verification of the higher thermal conductivity and thermal expansion coefficient of the samples prepared by the FHP sintering method. For example, the thermal conductivity of the Al-40Si composites sintered by the FHP method is higher than that of the conventional SPS method (139 to 107 W m<sup>-1</sup> K<sup>-1</sup>). These thermal performances of Al/Si composites are comparable with other Al/Si composites prepared by SPS methods. Given the economy of the FHP technique, it shows great potential for developing and producing Al matrix packaging materials via powder metallurgy sintering in the future.

**Author Contributions:** Conceptualization, J.J. and F.L.; data curation, H.D.; formal analysis, X.H., Z.L., W.Z. and Y.W.; funding acquisition: Y.L. (Yuanyuan Li); investigation, X.H.; methodology, J.J. and X.H.; project administration, F.L.; resources, Y.L. (Yuanyuan Li); supervision, F.L.; validation, Q.Z. and Y.L. (Yingru Li); writing—original draft, X.H.; writing—review and editing, Y.L. (Yingru Li). All authors have read and agreed to the published version of the manuscript.

**Funding:** This research was funded by the Science and Technology Plan Research Project of Hubei Education Department with grant No. Q20211905, the Science and Technology Program of Hubei Province with grant No. 2023AFB560 and the Open Fund of Key Laboratory of Green Manufacturing of Super-light Elastomer Materials of State Ethnic Affairs Commission, Hubei Minzu University with grant Nos. PT092002, PT092207, PT092210.

**Data Availability Statement:** The original data for this paper cannot be open-sourced to the public due to the commercial confidentiality involved.

**Acknowledgments:** The authors acknowledge the FHP-828 fast hot press sintering furnace provide by Haaten Technology Co. Ltd. (Suzhou, China).

**Conflicts of Interest:** The authors declare no conflict of interest.

## References

1. Mizuuchi, K.; Inoue, K.; Agari, Y. Trend of the development of metal-based heat dissipative materials. *Microelectron. Reliab.* **2017**, *79*, 5–19. [[CrossRef](#)]
2. Bahru, R.; Zamri, M.F.M.A.; Shamsuddin, A.H.; Shaari, N.; Mohamed, M.A. A review of thermal interface material fabrication method toward enhancing heat dissipation. *Int. J. Energy Res.* **2021**, *45*, 3548–3568. [[CrossRef](#)]
3. Wan, Y.-J.; Li, G.; Yao, Y.-M.; Zeng, X.-L.; Zhu, P.-L.; Sun, R. Recent advances in polymer-based electronic packaging materials. *Compos. Commun.* **2020**, *19*, 154–167. [[CrossRef](#)]
4. Zhang, S.; Xu, X.; Lin, T.; He, P. Recent advances in nano-materials for packaging of electronic devices. *J. Mater. Sci. Mater. Electron.* **2019**, *30*, 13855–13868. [[CrossRef](#)]
5. Wen, Y.; Chen, C.; Ye, Y.; Xue, Z.; Liu, H.; Zhou, X.; Zhang, Y.; Li, D.; Xie, X.; Mai, Y.-W. Advances on Thermally Conductive Epoxy-Based Composites as Electronic Packaging Underfill Materials—A Review. *Adv. Mater.* **2022**, *34*, 2201023. [[CrossRef](#)]
6. Yu, J.; Wang, C.; Shen, Q.; Zhang, L. Preparation and properties of Si/Al composites by spark plasma sintering. *Mater. Des.* **2012**, *41*, 198–202. [[CrossRef](#)]
7. Saraswat, E.; Maharana, H.; Murty, S.N.; Shekhar, S.; Kar, K.K.; Ramkumar, J.; Mondal, K. Fabrication of Al-Si controlled expansion alloys by unique combination of pressureless sintering and hot forging. *Adv. Powder Technol.* **2020**, *31*, 2820–2832. [[CrossRef](#)]
8. Zhai, W.-C.; Zhang, Z.-H.; Wang, F.-C.; Shen, X.-B.; Lee, S.-K.; Wang, L. Effect of Si content on microstructure and properties of Si/Al composites. *Trans. Nonferr. Met. Soc. China* **2014**, *24*, 982–988. [[CrossRef](#)]
9. Haque, A.; Shekhar, S.; Murty, S.N.; Ramkumar, J.; Kar, K.; Mondal, K. Fabrication of controlled expansion Al-Si composites by pressureless and spark plasma sintering. *Adv. Powder Technol.* **2018**, *29*, 3427–3439. [[CrossRef](#)]
10. Mizuuchi, K.; Inoue, K.; Agari, Y.; Nagaoka, T.; Sugioka, M.; Tanaka, M.; Takeuchi, T.; Tani, J.-i.; Kawahara, M.; Makino, Y. Processing of Al/SiC composites in continuous solid–liquid co-existent state by SPS and their thermal properties. *Compos. Part B Eng.* **2012**, *43*, 2012–2019. [[CrossRef](#)]
11. Sangha, S.; Jacobson, D.; Ogilvy, A.; Azema, M.; Junai, A.A.; Botter, E. Novel aluminium-silicon alloys for electronics packaging. *Eng. Sci. Educ. J.* **1997**, *6*, 195–201. [[CrossRef](#)]
12. Wang, F.; Xiong, B.; Zhang, Y.; Zhu, B.; Liu, H.; Wei, Y. Microstructure, thermo-physical and mechanical properties of spray-deposited Si–30Al alloy for electronic packaging application. *Mater. Charact.* **2008**, *59*, 1455–1457. [[CrossRef](#)]
13. Yu, K.; Li, C.; Yang, J.; Cai, Z.Y. Production and Properties of a 90%Si-Al Alloy for Electronic Packaging Applications. *Mater. Sci. Forum* **2009**, *610–613*, 542–545. [[CrossRef](#)]
14. Liu, J.; Xiu, Z.; Liang, X.; Li, Q.; Hussain, M.; Qiao, J.; Jiang, L. Microstructure and properties of Si/Al–20 wt% Si composite prepared by hot-pressed sintering technology. *J. Mater. Sci.* **2014**, *49*, 1368–1375. [[CrossRef](#)]
15. Gao, C.; Niu, L.; Ma, J.; An, Y.; Hu, Y.; Yang, L.; Chen, G.; Wang, Y. Al-50 wt% Si Alloy by Spark Plasma Sintering (SPS) for Electronic Packaging Materials. *J. Wuhan Univ. Technol. Mater. Sci. Ed.* **2022**, *37*, 500–506. [[CrossRef](#)]
16. Mizuuchi, K.; Inoue, K.; Agari, Y.; Tanaka, M.; Takeuchi, T.; Tani, J.I.; Kawahara, M.; Makino, Y.; Ito, M. Thermal conductivity of cubic boron nitride (cBN) particle dispersed Al matrix composites fabricated by SPS. In *Materials Science Forum*; Trans Tech Publications Ltd.: Stafa-Zurich, Switzerland, 2017; pp. 2413–2418.
17. Shu, S.; Yang, H.; Tong, C.; Qiu, F. Fabrication of TiCx-TiB2/Al Composites for Application as a Heat Sink. *Materials* **2016**, *9*, 642. [[CrossRef](#)]
18. Mizuuchi, K.; Inoue, K.; Agari, Y.; Tanaka, M.; Takeuchi, T.; Tani, J.-I.; Kawahara, M.; Makino, Y.; Ito, M. Effects of Bimodal and Monomodal SiC Particle on the Thermal Properties of SiC Particle-Dispersed Al-Matrix Composite Fabricated by SPS. *J. Metall. Eng.* **2016**, *5*, 1–12.
19. Tong, Z.; Shen, Z.; Zhang, Y. Aluminum/Diamond Composites and Their Applications in Electronic Packaging. In Proceedings of the 2007 8th International Conference on Electronic Packaging Technology, Shanghai, China, 14–17 August 2007; pp. 1–7.
20. Feng, H.; Yu, J.K.; Tan, W. Microstructure and thermal properties of diamond/aluminum composites with TiC coating on diamond particles. *Mater. Chem. Phys.* **2010**, *124*, 851–855. [[CrossRef](#)]
21. Jiao, Z.; Kang, H.; Zhou, B.; Kang, A.; Wang, X.; Li, H.; Yu, Z.; Ma, L.; Zhou, K.; Wei, Q. Research progress of diamond/aluminum composite interface design. *Funct. Diam.* **2022**, *2*, 25–39. [[CrossRef](#)]
22. Mizuuchi, K.; Inoue, K.; Agari, Y.; Morisada, Y.; Sugioka, M.; Tanaka, M.; Takeuchi, T.; Kawahara, M.; Makino, Y. Thermal conductivity of diamond particle dispersed aluminum matrix composites fabricated in solid–liquid co-existent state by SPS. *Compos. Part B Eng.* **2011**, *42*, 1029–1034. [[CrossRef](#)]
23. Mizuuchi, K.; Inoue, K.; Agari, Y.; Morisada, Y.; Sugioka, M.; Tanaka, M.; Takeuchi, T.; Tani, J.-I.; Kawahara, M.; Makino, Y. Processing of diamond particle dispersed aluminum matrix composites in continuous solid–liquid co-existent state by SPS and their thermal properties. *Compos. Part B Eng.* **2011**, *42*, 825–831. [[CrossRef](#)]
24. Mizuuchi, K.; Inoue, K.; Agari, Y.; Sugioka, M.; Tanaka, M.; Takeuchi, T.; Tani, J.-I.; Kawahara, M.; Makino, Y.; Ito, M. Bimodal and monomodal diamond particle effect on the thermal properties of diamond-particle-dispersed Al–matrix composite fabricated by SPS. *Microelectron. Reliab.* **2014**, *54*, 2463–2470. [[CrossRef](#)]
25. Yang, W.-S.; Xiu, Z.-Y.; Chen, G.-Q.; Wu, G.-H. Microstructure and thermal conductivity of submicron Si<sub>3</sub>N<sub>4</sub> reinforced 2024Al composite. *Trans. Nonferr. Met. Soc. China* **2009**, *19*, s378–s381. [[CrossRef](#)]
26. Mizuuchi, K.; Inoue, K.; Agari, Y.; Kawahara, M.; Makino, Y.; Ito, M. Thermal Properties of Al/ $\beta$ -SiC Composite Fabricated by Spark Plasma Sintering (SPS). *J. Metall. Eng.* **2014**, *3*, 59–68. [[CrossRef](#)]

27. Zhang, Y.; Li, J.; Zhao, L.; Zhang, H.; Wang, X. Effect of metalloid silicon addition on densification, microstructure and thermal-physical properties of Al/diamond composites consolidated by spark plasma sintering. *Mater. Des.* **2014**, *63*, 838–847. [[CrossRef](#)]
28. Sharma, N.K.; Misra, R.K.; Sharma, S. Modeling of thermal expansion behavior of densely packed Al/SiC composites. *Int. J. Solids Struct.* **2016**, *102–103*, 77–88. [[CrossRef](#)]
29. Cai, Z.; Wang, R.; Zhang, C.; Peng, C.; Wang, L. Microstructure and properties of Al/Sip composites for thermal management applications. *J. Mater. Sci. Mater. Electron.* **2015**, *26*, 4234–4240. [[CrossRef](#)]
30. Jia, Y.D.; Ma, P.; Prashanth, K.G.; Wang, G.; Yi, J.; Scudino, S.; Cao, F.Y.; Sun, J.F.; Eckert, J. Microstructure and thermal expansion behavior of Al-50Si synthesized by selective laser melting. *J. Alloys Compd.* **2017**, *699*, 548–553. [[CrossRef](#)]
31. Chong, G.; Li-Bin, N.; Lan, M.; Haoxuan, H.; Jun, M.; Yu-Jiao, A.; Yu-Yang, H. Effects of Spark Plasma Sintering Parameters on Microstructure and Properties of Al-50 wt.% Si Alloys. *Powder Metall. Met. Ceram.* **2022**, *60*, 556–566. [[CrossRef](#)]
32. Dhanashekar, M.; Kumar, V.S. Squeeze casting of aluminium metal matrix composites-an overview. *Procedia Eng.* **2014**, *97*, 412–420. [[CrossRef](#)]
33. Shabani, M.O.; Baghani, A.; Khorram, A.; Heydari, F. Evaluation of fracture mechanisms in Al-Si metal matrix nanocomposites produced by three methods of gravity sand casting, squeeze casting and compo casting in semi-solid state. *Silicon* **2020**, *12*, 2977–2987. [[CrossRef](#)]
34. Zhang, Q.; Zhang, H.; Gu, M.; Jin, Y. Studies on the fracture and flexural strength of Al/Sip composite. *Mater. Lett.* **2004**, *58*, 3545–3550. [[CrossRef](#)]
35. Dong, C.-G.; Wang, R.-C.; Chen, Y.-X.; Wang, X.-F.; Peng, C.-Q.; Jing, Z. Near-net shaped Al/SiCP composites via vacuum-pressure infiltration combined with gelcasting. *Trans. Nonferr. Met. Soc. China* **2020**, *30*, 1452–1462. [[CrossRef](#)]
36. Liao, J.; Chen, Z.; Guan, T.; Li, Y.; Xiao, Q.; Xue, L. High compression performance of Cf/SiC-Al composites fabricated by CVI and vacuum pressure infiltration. *Mater. Sci. Eng. A* **2021**, *811*, 141051. [[CrossRef](#)]
37. Liu, T.; He, X.; Zhang, L.; Liu, Q.; Qu, X. Fabrication and thermal conductivity of short graphite fiber/Al composites by vacuum pressure infiltration. *J. Compos. Mater.* **2014**, *48*, 2207–2214. [[CrossRef](#)]
38. Gupta, M.; Ibrahim, I.; Mohamed, F.A.; Lavernia, E. Wetting and interfacial reactions in Al-Li-SiC p metal matrix composites processed by spray atomization and deposition. *J. Mater. Sci.* **1991**, *26*, 6673–6684. [[CrossRef](#)]
39. Matizamhuka, W. Spark plasma sintering (SPS)-an advanced sintering technique for structural nanocomposite materials. *J. S. Afr. Inst. Min. Metall.* **2016**, *116*, 1171–1180. [[CrossRef](#)]
40. Tang, F.; Anderson, I.E.; Gnaupel-Herold, T.; Prask, H. Pure Al matrix composites produced by vacuum hot pressing: Tensile properties and strengthening mechanisms. *Mater. Sci. Eng. A* **2004**, *383*, 362–373. [[CrossRef](#)]
41. Zhang, L.; Wang, Z.; Li, Q.; Wu, J.; Shi, G.; Qi, F.; Zhou, X. Microtopography and mechanical properties of vacuum hot pressing Al/B4C composites. *Ceram. Int.* **2018**, *44*, 3048–3055. [[CrossRef](#)]
42. Zhang, Q.; Xiao, B.; Wang, D.; Ma, Z. Formation mechanism of in situ Al<sub>3</sub>Ti in Al matrix during hot pressing and subsequent friction stir processing. *Mater. Chem. Phys.* **2011**, *130*, 1109–1117. [[CrossRef](#)]
43. Xu, J.; Gao, B.; Kang, F. A reconstruction of Maxwell model for effective thermal conductivity of composite materials. *Appl. Therm. Eng.* **2016**, *102*, 972–979. [[CrossRef](#)]
44. Pietrak, K.; Wiśniewski, T.S. A review of models for effective thermal conductivity of composite materials. *J. Power Technol.* **2015**, *95*, 14–24.
45. Toptan, A.; Jiang, W.; Hales, J.D.; Spencer, B.W.; Casagrande, A.; Novascone, S.R. FEA-aided investigation of the effective thermal conductivity in a medium with embedded spheres. *Nucl. Eng. Des.* **2021**, *381*, 111355. [[CrossRef](#)]
46. Ventura, G.; Perfetti, M.; Ventura, G.; Perfetti, M. Electrical and Thermal Conductivity. In *Thermal Properties of Solids at Room and Cryogenic Temperatures*; Springer: Berlin/Heidelberg, Germany, 2014; pp. 131–168.
47. Leach, A. The thermal conductivity of foams. I. Models for heat conduction. *J. Phys. D Appl. Phys.* **1993**, *26*, 733. [[CrossRef](#)]
48. Drozdov, A.D.; deClaville Christiansen, J. Modeling thermal conductivity of highly filled polymer composites. *Polym. Eng. Sci.* **2019**, *59*, 2174–2179. [[CrossRef](#)]
49. Tu, H.; Ye, L. Thermal conductive PS/graphite composites. *Polym. Adv. Technol.* **2009**, *20*, 21–27. [[CrossRef](#)]
50. Warmuzek, M. *Aluminum-Silicon Casting Alloys: An Atlas of Microfractographs*; ASM International: Almere, The Netherlands, 2004.

**Disclaimer/Publisher’s Note:** The statements, opinions and data contained in all publications are solely those of the individual author(s) and contributor(s) and not of MDPI and/or the editor(s). MDPI and/or the editor(s) disclaim responsibility for any injury to people or property resulting from any ideas, methods, instructions or products referred to in the content.